doi:10.26443/seismica.v3i1.1185

Deep learning detects uncataloged low-frequency earthquakes across regions

Jannes Münchmeyer [*1], **Sophie Giffard-Roisin** [1], **Marielle Malfante** [2], **William B. Frank** [3], **Piero Poli** [4], **David Marsan**[1], **Anne Socquet** [1]

[1]Univ. Grenoble Alpes, Univ. Savoie Mont Blanc, CNRS, IRD, Univ. Gustave Eiffel, ISTerre, Grenoble, France, [2]Univ. Grenoble Alpes, CEA, List, Grenoble, France, [3]Department of Earth, Atmospheric and Planetary Sciences, Massachusetts Institute of Technology, Cambridge, MA, USA, [4]Dipartimento di Geoscienze, Università di Padova, Padova, Italy

Abstract Documenting the interplay between slow deformation and seismic ruptures is essential to understand the physics of earthquakes nucleation. However, slow deformation is often difficult to detect and characterize. The most pervasive seismic markers of slow slip are low-frequency earthquakes (LFEs) that allow resolving deformation at minute-scale. Detecting LFEs is hard, due to their emergent onsets and low signal-to-noise ratios, usually requiring region-specific template matching approaches. These approaches suffer from low flexibility and might miss LFEs as they are constrained to sources identified a priori. Here, we develop a deep learning-based workflow for LFE detection and location, modeled after classical earthquake detection with phase picking, phase association, and location. Across three regions with known LFE activity, we detect LFEs from both previously cataloged sources and newly identified sources. Furthermore, the approach is transferable across regions, enabling systematic studies of LFEs in regions without known LFE activity.

Production Editor: Gareth Funning
Handling Editor: Jack Muir
Copy & Layout Editor: Abhineet Gupta

Signed reviewer(s): David Shelly

Received: January 18, 2024
Accepted: April 10, 2024
Published: May 10, 2024

Non-technical summary Earthquakes are caused by sudden movements on tectonic faults. While such sudden movements have been documented for thousands of years, the last decades have revealed that tectonic faults also host a wide range of slow deformation. Such slow slip happens over the scale of days to years but is still substantially faster than regular plate convergence rates. Recent years have shown that slow slip can play an essential role in the buildup of large earthquakes. Classically, slow deformation is detected and characterised using geodetic observations, such as GNSS or InSAR. This limits the time and space resolution. An alternative is looking for seismic markers accompanying slow slip, among which the most pervasive are low-frequency earthquakes (LFE). Due to their low signal to noise ratio and emergent onsets, such LFEs are notoriously difficult to detect. Here, we develop a novel method for detecting LFEs using deep learning. Our method successfully detects LFEs from both known and unknown sources. In contrast to previous approaches, our method can detect LFEs without prior knowledge of the region, which makes it promising for LFE detection in regions where no LFEs have been found previously.

1 Introduction

Stress release on tectonic faults can happen in two ways: fast and slow. Fast deformation happens in the form of earthquakes; slow relaxation is observed as creep or episodes of accelerated slip, so-called slow slip events (Dragert et al., 2001; Ozawa et al., 2002; Lowry et al., 2001; Ide et al., 2007a). The complex interactions between fast and slow deformation might be at play during the initiation of large earthquakes (Radiguet et al., 2016; Socquet et al., 2017; Cruz-Atienza et al., 2021). However, studying these interactions requires detailed catalogs of both deformation types. While the impulsive nature of earthquakes causes clear signatures on seismic recordings, detecting slow slip is substantially more challenging. Its detection commonly uses geodetic observations with a limited spatial and temporal resolution (Michel et al., 2019; Okada et al., 2022; Costantino et al., 2023).

An alternative way to map slow deformation is by detecting and characterising its seismic markers. One such type of markers are low-frequency earthquakes (LFEs), weak seismic signals with a duration on the scale of seconds. Recent research shows that the rate and magnitude of LFEs track the slow deformation (Frank and Brodsky, 2019; Mouchon et al., 2023). LFEs are similar to regular earthquakes in some characteristics, e.g., distinct phase arrivals or predominantly double-couple sources, but also have clear differences (Shelly et al., 2007; Ide et al., 2007b; Royer and Bostock, 2014; Imanishi et al., 2016; Supino et al., 2020; Wang et al., 2023). First, they have an eponymous depletion of energy in the high-frequency band (above a few Hz). Second, in consequence of missing high frequencies, they do not exhibit impulsive arrivals but are emergent, making them hard to detect. Third, they often occur in intense bursts with inter-event times of only seconds, leading to superimposed waveforms commonly referred to as tremors (Shelly et al., 2007).

To illustrate the challenges these characteristics cause for LFE detection, it is worth contrasting LFE detection with the identification of regular earthquakes.

*Corresponding author: munchmej@univ-grenoble-alpes.fr

Detecting regular earthquakes traditionally relies on a two-step procedure: (i) phase picking, i.e., identifying P and S waves arrival times at seismic stations; (ii) phase association, i.e., selecting sets of picks across stations that are consistent with a common source location and origin time. Downstream analysis can then determine the event location and additional source parameters. In this workflow, a side benefit of the phase association step is that it acts as a quality control to remove spurious phase picks. At the moment, such a workflow is usually not applicable to LFE detection, as the low signal-to-noise (SNR) ratio and the emergent onsets make it impossible for classical algorithms to pick phase arrivals. There are exceptions, notably the JMA catalog (Japan Meteorological Agency, 2023), but these rely on high-quality and high-density data, manual intervention, and high SNR LFEs. Instead, LFE detection usually relies on manual identification (Shelly, 2010), beamforming (Frank and Shapiro, 2014), or phase coherence (Gombert and Hawthorne, 2023). These approaches often suffer from high computational demand or requirement for manual labour. However, they can be used to generate LFE template waveforms forming an initial catalog for a subsequent matched filtering search on long running recordings. As the initial approaches often fail to identify all existing LFE sources, such catalogs will be biased towards certain sources.

Due to its high sensitivity, matched filtering, also known as template matching, has become the de facto standard for LFE detection (Shelly, 2017; Bostock et al., 2015; Frank et al., 2014). Once initial templates are identified, the method identifies repeat occurrences of the template events by correlating these with the continuous waveforms. In addition to detecting occurrences, this procedure groups the LFEs into families according to their matching templates. This allows to stack waveforms and accurately locate the families. While highly sensitive, matched-filtering presents several disadvantages: templates are always region and station specific, matched filtering does not provide locations for individual events, and the model can not detect LFEs outside the initially detected families. Especially the last limitation shapes our understanding of LFEs, as template matching can only recover repeating events, potentially skewing our view of overall LFE behavior by the most repetitive sources. Furthermore, the grouping into families is partially artificial, as template matches often overlap, i.e., many detections can not be uniquely assigned to one family.

A closely linked task to the detection of LFEs is the detection of tectonic tremors. Typical methods leverage either coherency across station, through source scanning (Kao et al., 2005), waveform coherency (Armbruster et al., 2014), envelope correlations (Bombardier et al., 2023), or repetitiveness of waveform motives within or across stations (Rubin and Armbruster, 2013). However, while the underlying processes are closely related, the tasks pose distinct challenges. Tremors are usually several minutes long, making them easier to detect than LFEs. In addition, these longer waveforms make it easier to locate them, as more characteristics, e.g., envelopes, can be used for location. In contrast, LFEs are short signals, with waveforms lasting at most a few seconds, making detection and location more difficult. However, the short duration of LFEs also implies that they can monitor underlying processes at a higher resolution than tremors, thereby providing additional insights into slow deformation. In some cases, waveform coherency methods similar to tremor detection can be applied for LFE detection, but the results are usually restricted to high signal-to-noise ratio examples (Savard and Bostock, 2015).

To build a flexible LFE detector addressing the disadvantages of template matching, it would be appealing to make a more traditional earthquake detection workflow applicable to LFEs. The critical point for this is a viable automatic phase picker for LFE arrivals. We borrow from the recent breakthroughs in seismic phase picking with deep learning, where recent neural network models have substantially improved earthquake detection (Zhu and Beroza, 2019; Ross et al., 2018; Münchmeyer et al., 2022). These neural network models are trained on millions of manually labelled phase arrivals and thereby learn to accurately discern seismic phase arrivals from noise and accurately determine arrival times. The application of these models to continuous data has allowed to substantially increase the completeness of earthquake catalogs (Tan et al., 2021; González-Vidal et al., 2023; Moutote et al., 2023).

For tremor and LFE detection with deep learning, only few studies exist. Rouet-Leduc et al. (2020) identify tremor episodes in single-station records, but do not attempt to detect or locate individual LFEs. Thomas et al. (2021) focus on LFEs on the San Andreas fault and test model configurations on cataloged events. The preprint of Lin et al. (2023) presents an LFE detection workflow similar to the one presented here but focus exclusively on Southern Vancouver Island. Here, we develop a deep learning based LFE picker and show its applicability to three independent study regions: Cascadia, Guerrero and Nankai. To train our picker, we develop a novel strategy for synthetic data generation that allows for fine-grained control of the training process. Using this method, we set up a classical earthquake detection workflow and demonstrate how to automatically create LFE catalogs across different world regions. Our model successfully identifies and locates individual LFEs, even without using any training examples from the target region. The resulting catalogs are coherent with classical catalogs but have been obtained in a fully automated and region-agnostic manner. Furthermore, the catalogs identify LFEs missing from the reference catalogs, showing that our approach can uncover sources missed in the template matching procedures. We make the trained picker available with a user-friendly interface through SeisBench (Woollam et al., 2022).

2 Training and validation of a deep learning LFE phase picker

For detecting LFEs and determining their phase arrival times, we build a deep learning network. Our network is closely modeled after PhaseNet (Zhu and

Beroza, 2019) due to the model's simplistic architecture and the excellent performance on earthquake data (Münchmeyer et al., 2022). PhaseNet is a 1D U-Net, i.e, a neural network consisting of convolutional encoder and decoder branches and skip connections (Ronneberger et al., 2015). We provide the model with 60 s of 3-component waveforms sampled at 20 Hz, bandpass-filtered between 1 and 8 Hz, the band in which LFEs are typically observed. The model outputs probability curves for P and S phase arrivals. We provide full details on the model and training procedure in the supplement.

In contrast to traditional earthquake pickers, training the model on cataloged LFE waveforms is suboptimal. First, LFEs occur in bursts, i.e., around one LFE arrival there are often further arrivals many of which have not been labelled. This leads to incorrect labelling and in addition makes a quantitative analysis of the model performance difficult. Second, most LFE catalogs are based on template matching, i.e., individual arrivals need to be inferred from arrival times on templates. Due to the low SNR, these times are often highly inaccurate, leading to high model uncertainties. Instead, we train our model on synthetics. For this, we combine LFE stacks with real seismic noise, allowing us to control the number and timing of LFEs and the SNR (Figure 1). We use up to three LFEs per trace to train the model to recognise events with low inter-event times. We use seismic noise from the INSTANCE dataset for Italy (Michelini et al., 2021) as it contains no known LFEs.

We train our model using four regions: Southern Vancouver Island in Cascadia (Canada/USA) (Bostock et al., 2015), the central section of the San Andreas fault (USA) (Shelly, 2017), Guerrero (Mexico) (Frank et al., 2014), and Nankai (Japan) (Japan Meteorological Agency, 2023). Figure S1 shows the distribution of events and stations in the reference catalogs. For Cascadia, San Andreas and Guerrero, we use template matching catalogs and the previously described strategy for generating examples. For Nankai, we apply the classical training scheme as used for earthquakes as individual picks are available. Further details on the datasets can be found in the supplement.

We evaluate our trained models quantitatively on synthetic examples generated with the previously described noise plus stack strategy. The performance on synthetic data can serve as a proxy for the expected performance on real data. We exclude the Nankai catalog from the analysis, because the catalog incompleteness precludes the extraction of challenging yet guaranteed LFE-free time windows. As this study focuses on the generated LFE catalogs, we only provide a synopsis of the analysis on synthetics here and refer to the supplement for further details.

Overall, the models show excellent detection performance for both P and S waves, with an area under the curve (AUC) of the receiver operator characteristics of 0.97 to 1.00 in all regions for positive SNR in dB scale (Figure 1). The performance degrades mildly at -2.5 dB SNR and more sharply after, but all AUC values stay above 0.88 even at -10 dB SNR. Models transfer well across regions with the worst results for a model trained exclusively on Cascadia (Figure S2). The best performing model is the one trained jointly on all four regions. Therefore, we use the model trained jointly on all regions in the subsequent analysis unless explicitly stated otherwise.

Analysing the pick time residuals, clear regional differences are visible, with lowest residuals in Cascadia (Figure S3). In all regions, average residuals are about 0.3 s larger for P arrivals than S arrivals, indicating that these are more difficult to pick. With standard deviations between 0.3 and 1.3 s (at 0 dB), residuals are substantially higher than for traditional earthquake pickers (Münchmeyer et al., 2022). Nonetheless, the residuals expose only low or no bias across all regions. For the regional differences in performance, we think that they can primarily be attributed to the heterogeneity in data quality and SNR. For example, the Cascadia stacks show the highest SNR, leading to the lowest pick residuals. In turn, this implies that no conclusions about inherent regional differences in difficulty for picking LFEs can be inferred.

3 Building deep learning LFE catalogs

Using our phase picking model, we set up an LFE catalog workflow similar to the classical earthquake detection workflow. Here we provide an overview of the workflow with further details in the supplement. First, we pick P and S phases by applying the trained deep learning model to continuous waveforms using SeisBench (Woollam et al., 2022). Second, we use the PyOcto phase associator (Münchmeyer, 2024) to identify coherent arrivals across stations. Third, we use NonLinLoc (Lomax et al., 2000) with a 1D velocity model to perform absolute location of the events. To avoid false detections, we filter the events based on the number of phase picks and the location residuals. For comparison, we create earthquake catalogs using the same waveforms and workflow but using a PhaseNet model trained on INSTANCE implemented in SeisBench as the picker (Zhu and Beroza, 2019; Michelini et al., 2021; Woollam et al., 2022).

As we observed a certain number of events detected as both earthquakes (EQs) and LFEs, we remove these events from the LFE catalogs (Figure S4). We note that it is not clear whether these events should be classified as LFEs or EQs. The level of overlap is dependent on the region, with almost no overlap in Cascadia and Guerrero, a 5% overlap on the San Andreas fault, and a 40% overlap in Nankai. While we are not certain what causes this different behavior, we speculate that in Nankai, LFEs and earthquakes show a wide range of apparent spectra, due to the diverse event distribution and frequency dependent attenuation. This might lead to a higher number of overlapping detections.

We apply our workflow to compile LFE catalogs for the four study regions. As we focus on studying the performance of the model and its resulting catalogs, we restrict ourselves to short study periods: 2003-02-26 to 2003-03-10, 2004-07-02 to 2004-07-27, and 2005-09-03 to 2005-09-25 for Cascadia; 2005-09-01 to 2005-11-30 for Guerrero; 2014-07-01 to 2014-10-01 for San Andreas; 2012-05-25 to 2012-06-14 for Nankai. We chose the pe-

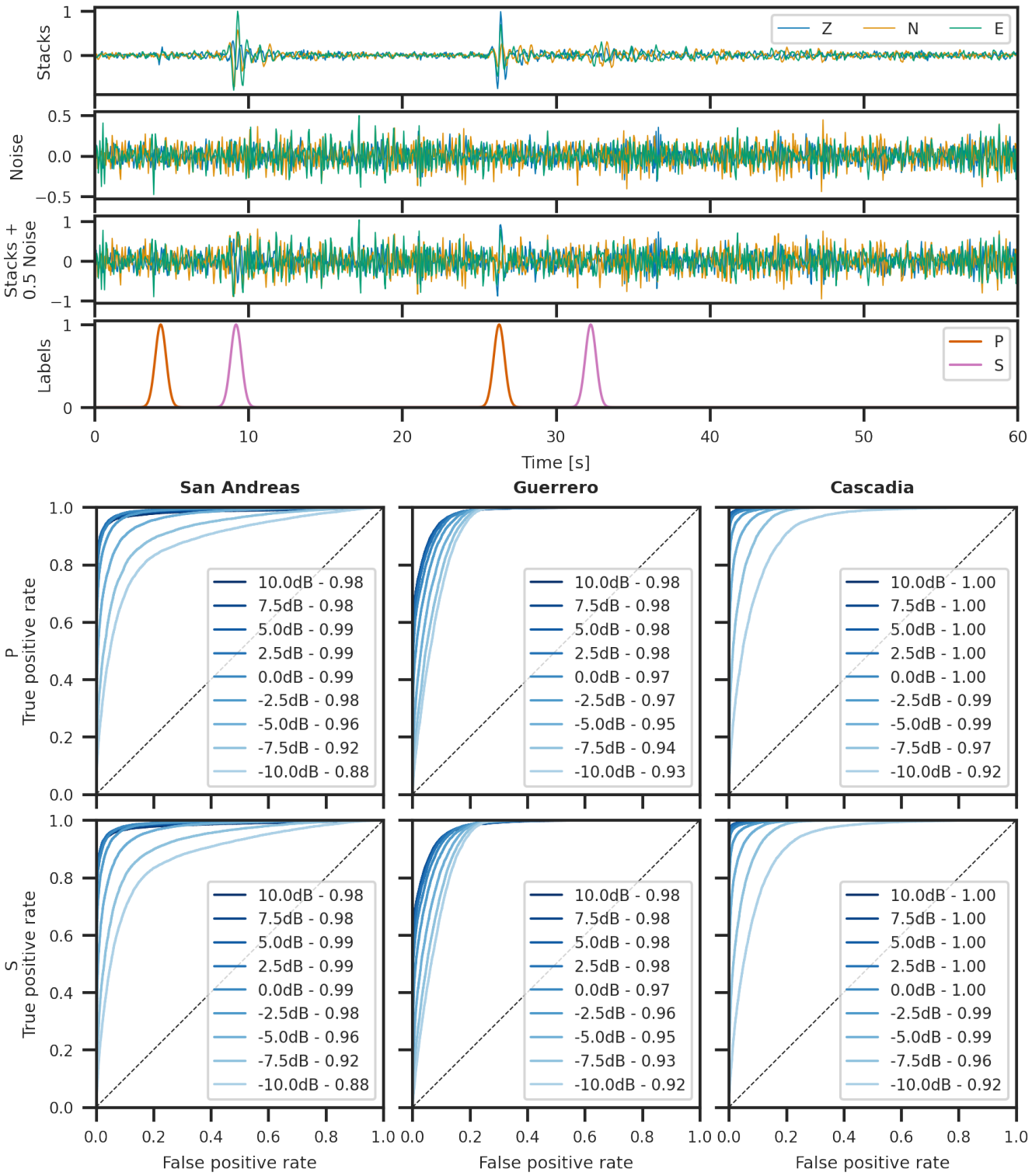

Figure 1 Data generation procedure and evaluation results for synthetic data. The top panels show (top to bottom): the combination of two LFE stacks from Cascadia, a 60 s noise segment from INSTANCE, the combination of signal and noise at 3 dB SNR, and the Gaussian pulse labels for the P and S arrivals. The bottom panels show the receiver operating characteristics (ROC) at different SNR. The numbers in the legend indicate the area under the ROC curve (AUC). For all plots, we use the joint model trained on all four datasets.

riods to contain both intense LFE activity and segments without any identified LFEs.

Figure 2 shows the spatial event distributions. While the overall event locations are scattered, we notice strong similarities with the reference catalogs. For Cascadia (10211 events detected), LFE activity is distributed along a band underneath South Vancouver island. For Guerrero (876 events detected), LFEs occur mostly in a band between 100° and 99° West and around 18.25° North. For Nankai (2525 events detected), a clear band of LFEs is visible in Southwestern Nankai. Further LFEs around 135.5° E match the second band of LFEs com-

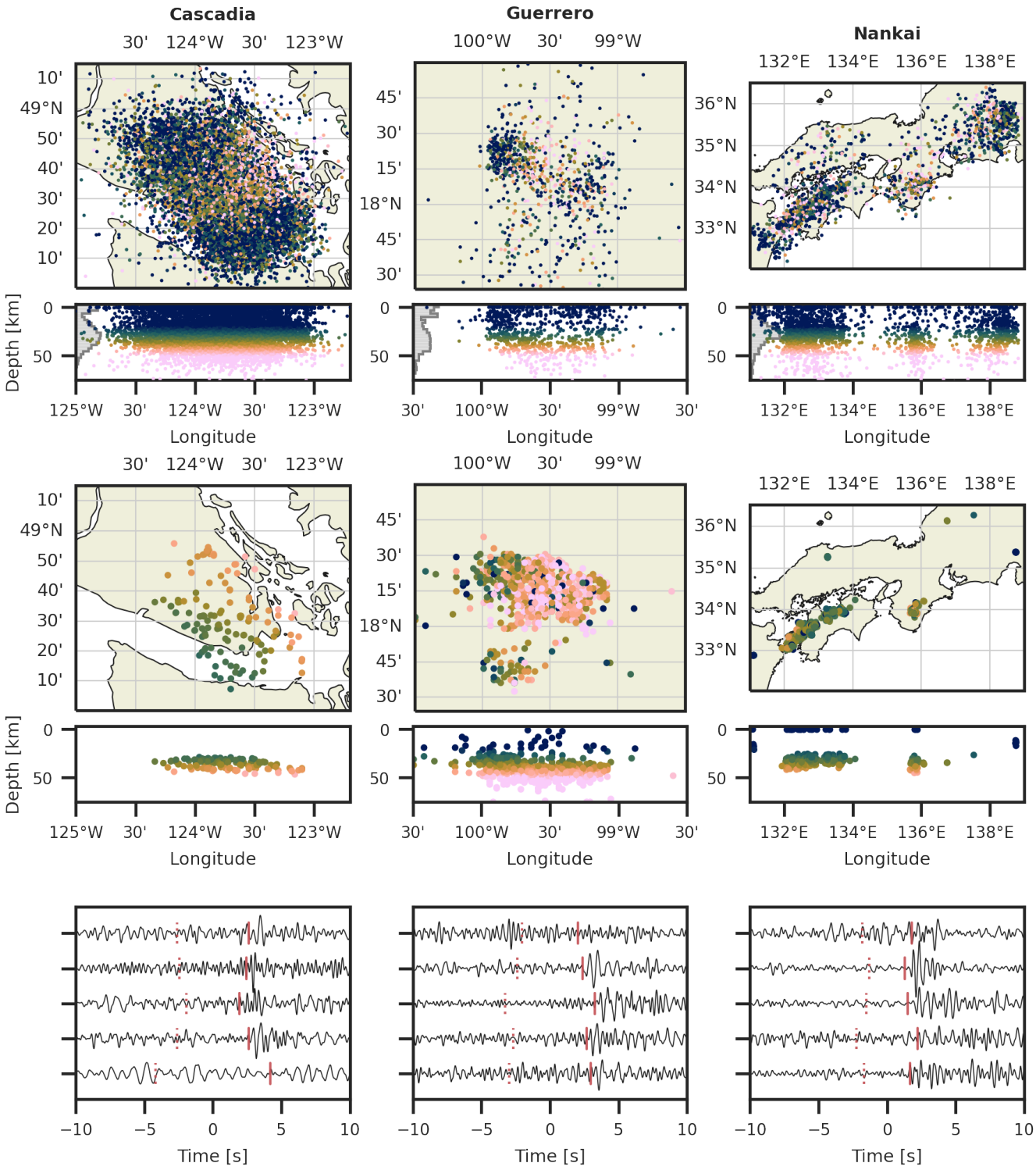

Figure 2 LFE catalogs obtained from deep learning (top row) and the reference catalogs (middle row). For deep learning, each dot represents one LFE. The bottom subpanels show depth cross-sections, showing longitude and depth of events. Color encodes event depth. The histograms on the left of the cross-section show the depth distribution of the detected events. In the reference catalogs for Cascadia (Bostock et al., 2015) and Guerrero (Frank et al., 2014) each dot represents an LFE family. For Nankai (Japan Meteorological Agency, 2023) individual LFEs are plotted. The bottom panels show waveforms of associated LFE picks from deep learning in each region. Red lines indicate phase picks (dotted for P, solid for S).

monly observed in Nankai. For San Andreas (975 events detected), the new catalog deviates from the previous observations, with the detection broadly distributed in space instead of along the fault (Figure S7). This is likely caused by very poor locations due to the station geometry. As many events are only detected by the Parkfield borehole array with very dense station spacing, the aperture is small. Together with high pick uncertainties, this makes determining accurate locations challenging. Therefore, we will exclude San Andreas from

the following analysis.

In all catalogs, the event depth exposes high scatter. Nonetheless, the largest density of events is around the previous estimates of LFE source depths. For Cascadia, events within the network show less scatter on depth than outside the network. We suggest that this is caused by the high timing uncertainty of the picks. In particular, a high P pick uncertainty will cause poor depth constraints as the P to S time is indicative of depth. Template matching catalogs alleviate this problem by locating LFE families instead of single events. In Guerrero, we observe an arc-shaped depth distribution. This is most likely related to the station distribution that traces out almost a straight line, leading to poor location constraints perpendicular to the station line (Frank and Shapiro, 2014).

Figure S5 shows the event density of the detected events. This visualisation further highlights the match with the reference catalogs both in terms of latitude and longitude and in terms of depth. For Japan, the highest event density occurs in the South-Western band of LFE activity. For Cascadia, the fine structure of detected LFEs is compatible with earlier publications, e.g., clear overlap is visible with patches A and C in the visualisation of LFE density of Figure 7 by Savard and Bostock (2015).

Even though the overall shape of the catalogs is consistent with the previous catalogs, this alone does not confirm that the identified events are indeed LFEs. We therefore conduct additional analysis into the newly obtained catalogs. Figure 3 shows spatial and temporal patterns in the catalogs. In Cascadia, LFEs in all three observed sequences show a clear North-Westward migration. This is consistent with the slow slip and tremor migration patterns in the area during these episodes (Wech, 2021). We conducted an additional analysis, comparing the PNSN tremor catalog and LFEs detected using our method for a 31 day period in 2021 (Figure S6). This analysis shows a high agreement between LFE and tremor locations, density, and temporal development. This holds even though for this time period we used a less dense station coverage and considered a larger part of Vancouver Island than in the 2003 to 2005 episodes.

For Nankai, we observe a migration in the North-Eastward direction. Notably, the migration is not continuous but rather has a gap and an additional, earlier cluster at the far North-West. This pattern matches exactly the migration pattern in the JMA catalog. We do not observe clear spatial migration patterns in Guerrero, however, such patterns have previously only been identified with very precise location estimates (Frank et al., 2014). In all regions, the evolution of daily event rate between the deep learning and reference catalogs is highly similar with Pearson correlation coefficients between 0.74 and 0.93. In absolute numbers, the deep learning method detects substantially fewer events than the template matching, but more events than the manual detection procedure of the JMA. We note that the number of events from deep learning is highly dependent on the chosen quality control parameters, which we set rather conservatively to avoid false positive detections.

Figure 4 shows a comparison of the velocity spectra of LFEs detected by our method, earthquakes and noise in the three regions. The spectra clearly show the characteristics of the different event types. The earthquake spectra show increasing or at least constant energy up to about 10 Hz. In contrast, the LFEs show a continuous decrease or at most constant levels of energy from low frequencies onward. The LFEs only show substantially higher energy than the noise in a small frequency band, while the EQs show substantially higher SNR at high frequencies. This depletion in energy at higher frequencies is the key property of LFEs.

4 Increased diversity of LFE sources through deep learning

We compare the detected events to the reference catalogs (Figure S8). In Cascadia, for 64% of the LFEs from our workflow, we find an LFE in the reference catalog within 10 s; for Guerrero for 81% of the events. For Nankai, only 8% of our LFEs are in the reference catalog, however our catalog also substantially exceeds the original catalog in the total number of events. Conversely, we recover 39% of the cataloged events. Note that a loose threshold for matching is justified due to uncertainties in the origin times due to inaccurate locations. On one hand, these results are another confirmation that the method correctly identifies LFEs. On the other hand, the substantial fraction of uncataloged events suggests that our method identifies previously unidentified LFEs. In the following, we verify and analyse these detections.

First, we rule out spurious detection. To this end, we scramble the picked arrival times of each station by applying small random shifts. We choose constant shifts for each station for every hour. This destroys the exact times, while keeping the pick distribution, the P to S times within a station, and the higher number of picks within tremor bursts intact. We then build "catalogs" by associating these scrambled pick times, using the same associator settings as for the actual catalogs. The scrambled "catalogs" only contain about 5% to 10% of the number of events contained in the original catalogs and show no spatial coherence (Figure S10). Even these numbers are still likely an overestimation of the false positive rate, as events recorded at many stations are likely to be unperturbed by our scrambling procedure. Therefore, at least 20% additional detections can not be attributed to spurious associations.

Mapping the events without matches in the reference catalog (Figure S11) reveals that they follow the same spatial extent and migration pattern as the full catalog. Notably, for Cascadia and Mexico there are changes in the temporal patterns. For Cascadia, the newly detected events concentrate early and late in the LFE sequence, coinciding with a spatial location around the southeastern tip of Vancouver island and towards the northwestern end of the LFE cluster. Nonetheless, there are additional detections dispersed throughout the whole region including the central region with good coverage in the reference catalog. For Mexico, the largest frac-

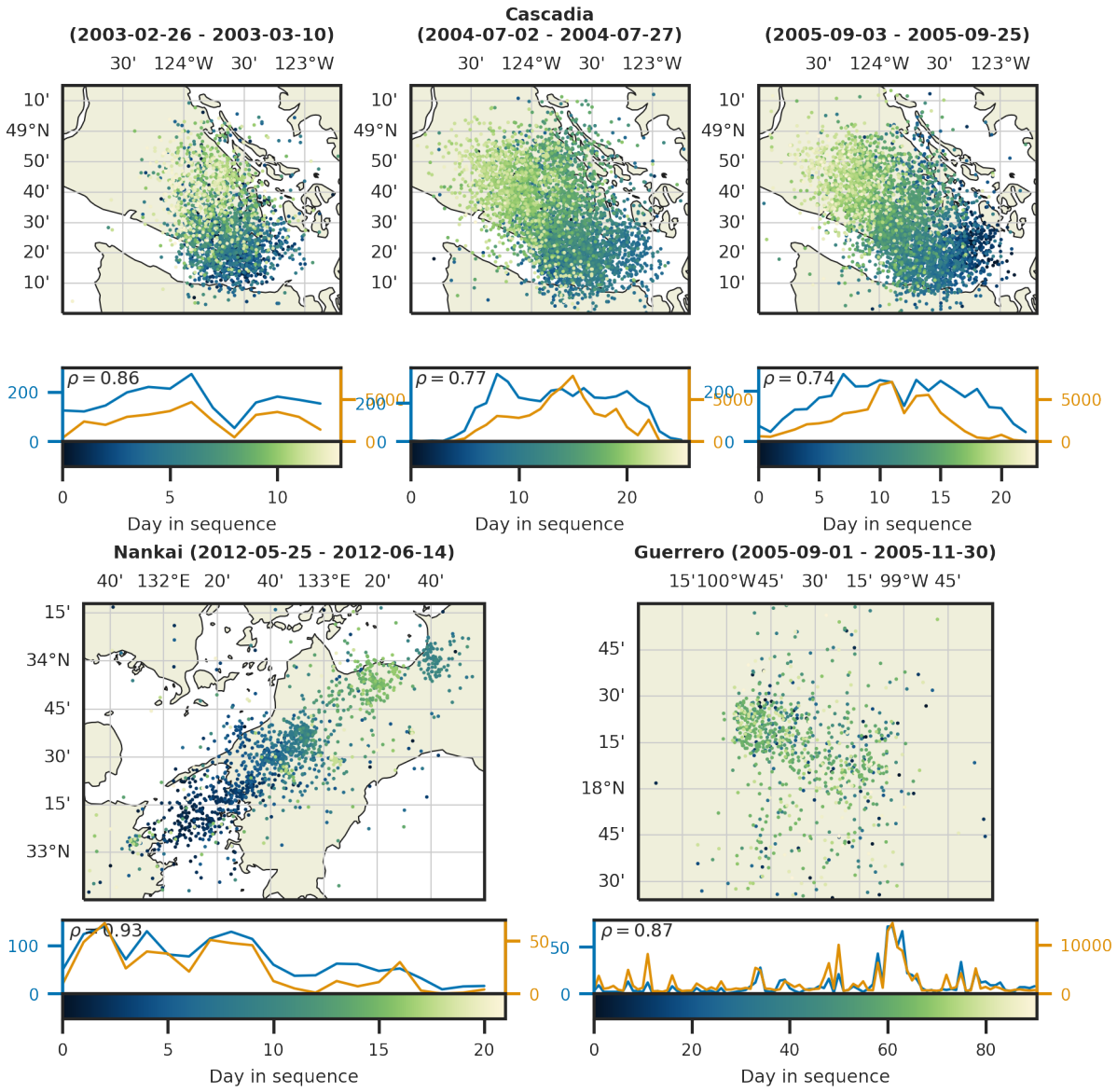

Figure 3 Spatial and temporal migration patterns of detected LFEs. Each dot represents one LFE. The time within the sequence is indicated by colour. The bottom panel shows the number of events per day for the LFEs from deep learning (blue) and reference catalogs (orange). The numbers in the upper left corners indicate the Pearson correlation coefficient between the daily number of events between the two catalogs.

tion of new detections clusters in time between days 30 and 50 of the analyses sequence. Visualising the interevent time (Figure 4) confirms these observations. Both the full deep learning catalogs and the catalog of events without a match in the reference catalogs show clear burst behaviour. In particular for Mexico, certain LFE bursts are contained virtually completely in the template matching catalog, while others have not been identified at all. This highlights that the newly detected LFEs do not only uncover new sources but even new LFE bursts.

To further validate this finding, we correlate the uncataloged detections with the family stacks from the reference catalogs (Figure S12). For Cascadia, the distribution of correlation values for these uncataloged detections are identical to the noise distribution, i.e., the new detections do not match known sources. For Guerrero, some events show systematically higher correlations than the noise. Nonetheless, the vast majority of our additional detections do not match the known sources any better than the noise. This verifies that these new detections are systematically different and that these events can not be found with template matching without identifying further, novel templates.

Extending upon the finding that the model can generalise from known families to LFEs outside these families, we investigate the ability to detect LFEs in regions the model has not been trained on. For this analysis, we trained leave-one-out models, i.e., models trained on all but one region, and applied them on the left-out region. Figure S13 visualises the spatial and temporal migration patterns. Again, the clear migration patterns in Nankai and Cascadia are retrieved. Furthermore, the number of events correlates highly (Pearson correlation between 0.69 and 0.82) with the reference catalogs. The total size of the catalogs varies, with a substantially

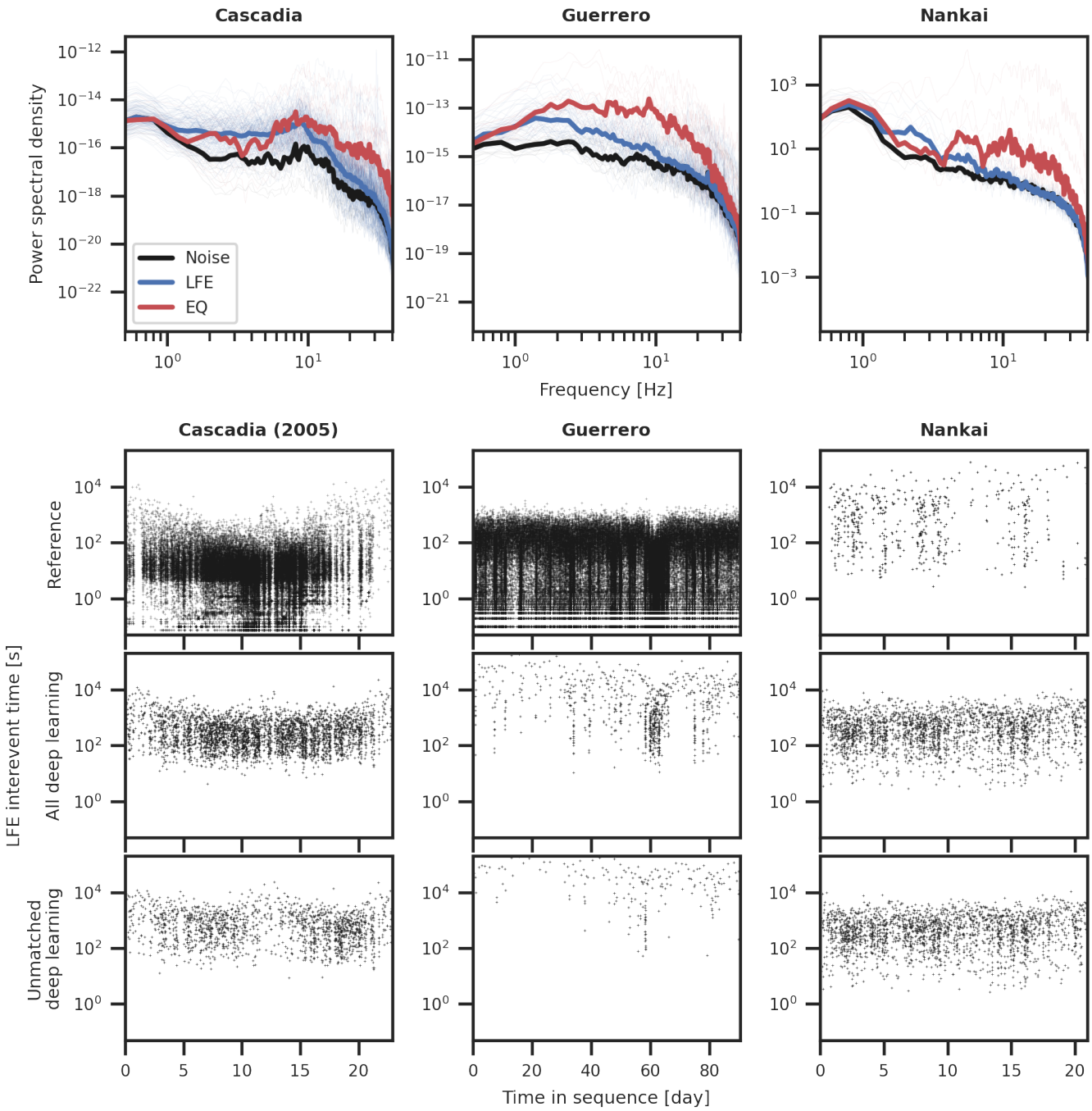

Figure 4 Spectra and interevent times in the different regions. The top part shows velocity power spectral density for noise, earthquakes (EQs), and LFEs detected using deep learning. For each region, all traces stem from one reference station (Cascadia - MGCB, Guerrero - MAXE, Nankai - IIDH). Noise example have been extracted outside tremor episodes. Spectra have been calculated from the horizontal components (20 s windows for noise, 11 s windows starting 1 s before the S arrival for events). Thin lines show individual spectra, bold lines median spectra. EQs were selected at a similar distance and depth range to the LFEs. Network averaged spectra are shown in Figure S9. The bottom part shows the development of interevent times during the LFE sequences in the reference catalogs, the deep learning catalogs, and for the unmatched events, i.e., all events from the deep learning catalogs that are not in the reference catalogs. Vertical stripes in the events indicate the occurrence of LFE bursts. For Cascadia, we only visualise the 2005 sequence for simplicity. We visualise all events from the reference catalogs without further declustering, leading to very low interevent times.

smaller catalog in Cascadia, a similarly-sized catalog in Nankai, and a far bigger catalog in Guerrero. However, these might be related to changes in the model confidence values rather than their actual quality as we produced all catalogs with fixed picking thresholds. The cross-regional analysis clearly illustrates that the models can be transferred across regions and recover LFEs from families they have not been trained on.

5 Conclusion

Our analysis shows that deep learning and template matching are complementary in the way they detect LFEs with specific advantages and disadvantages for either method. The biggest strength of deep learning is the flexibility. The model can be applied to additional stations, including temporary stations, shows higher diversity in terms of event families, and can be transferred across regions. In addition, our method directly allows to locate single LFEs, even though with substantial uncertainties in terms of depth. In contrast, template matching requires a predefined set of sources that is difficult to obtain and specific to each region and set of stations. While rigid, this leads to a more sensitive model, as evidenced by higher event counts. Furthermore, it allows template matching to identify LFEs with fewer stations than deep learning. For LFEs, commonly no individual location is performed after template matching, due to the difficulties caused by the low SNR ratio. However, it has been shown that relative locations of individual LFEs can be determined with classical methods as well (Shelly et al., 2009). A promising avenue might be the combination of deep learning and template matching, i.e., using deep learning to identify a diverse set of templates and afterwards use template matching to increase the completeness of the identified families.

Lastly, the deep learning method extends our view of LFEs by detecting previously unidentified sources. Building a comprehensive set of templates for template matching is challenging: the low bandwidth and SNR makes it difficult to distinguish between closely spaced sources, leading to a trade-off between missing sources and redundant templates. In contrast, the deep learning method is source-agnostic, i.e., no selection of sources needs to be performed for detecting individual events. Such a source-agnostic view is necessary to perform unbiased subsequent analysis that requires a complete view of LFE sources, such as estimates of slow slip. In addition, the fact that the model can be transferred across regions shows that LFEs have universal, region-independent properties similar to earthquakes. Given our results, we expect that deep learning methods will allow to map LFEs across world regions with high consistency and diversity.

Acknowledgements

We thank David Shelly for sharing his data on the San Andreas LFE catalog and for his insightful comments on the manuscript. We thank Jack Muir and an anonymous reviewer for their comments that helped improve the manuscript. We thank Albanne Lecointre for help with processing the FNet data. This work has been supported by MIAI@Grenoble Alpes (ANR-19-P3IA-0003). This work has been partially funded by the European Union under the grant agreement n°101104996 ("DECODE") and the ERC CoG 865963 DEEP-trigger. Views and opinions expressed are however those of the authors only and do not necessarily reflect those of the European Union or REA. Neither the European Union nor the granting authority can be held responsible for them. This work was granted access to the HPC/AI resources of IDRIS under the allocation 2022-AD011012345R1 made by GENCI.

Data and code availability

The stack data sets for Cascadia, San Andreas, and Guerrero are available through SeisBench (https://github.com/seisbench/seisbench, https://doi.org/10.5281/zenodo.5568812) from version v0.7 onwards. The model including pretrained weights is available through SeisBench starting from the same version. The INSTANCE noise dataset is available through SeisBench and at https://doi.org/10.13127/instance. The PNSN tremor catalog is available at https://pnsn.org/tremor/. The FNet data is available from the NIED at https://www.fnet.bosai.go.jp/. We use waveforms from the BK (Northern California Earthquake Data Center, 2014a), BP (Northern California Earthquake Data Center, 2014b), CI (California Institute of Technology and United States Geological Survey Pasadena, 1926), CN (Natural Resources Canada, 1975), C8 (Natural Resources Canada, 2002), NC (USGS Menlo Park, 1966), PB (UNAVCO, United States of America, 2004), PO (Geological Survey of Canada, 2000), TA (IRIS Transportable Array, 2003), and TO (MASE deployment; Caltech, 2007) networks. Waveforms were accessed through the IRIS and NCEDC FDSN webservices, and from the PNSN.

Competing interests

The authors have no competing interests.

References

Armbruster, J. G., Kim, W.-Y., and Rubin, A. M. Accurate Tremor Locations from Coherent S and P Waves. *Journal of Geophysical Research: Solid Earth*, 119(6):5000–5013, 2014. doi: 10.1002/2014JB011133.

Bombardier, M., Dosso, S. E., Cassidy, J. F., and Kao, H. Tackling the Challenges of Tectonic Tremor Localization Using Differential Traveltimes and Bayesian Inversion. *Geophysical Journal International*, 234(1):479–493, July 2023. doi: 10.1093/gji/ggad086.

Bostock, M. G., Thomas, A. M., Savard, G., Chuang, L., and Rubin, A. M. Magnitudes and Moment-Duration Scaling of Low-Frequency Earthquakes beneath Southern Vancouver Island. *Journal of Geophysical Research: Solid Earth*, 120(9):6329–6350, 2015. doi: 10.1002/2015JB012195.

California Institute of Technology and United States Geological Survey Pasadena. Southern California Seismic Network, 1926. doi: 10.7914/SN/CI.

Caltech. Meso America Subduction Experiment, 2007. doi: 10.7909/C3RN35SP.

Costantino, G., Giffard-Roisin, S., Radiguet, M., Dalla Mura, M., Marsan, D., and Socquet, A. Multi-station deep learning on geodetic time series detects slow slip events in Cascadia. *Communications Earth & Environment*, 4(1):435, 2023. doi: 10.1038/s43247-023-01107-7.

Cruz-Atienza, V. M., Tago, J., Villafuerte, C., Wei, M., Garza-Girón, R., Dominguez, L. A., Kostoglodov, V., Nishimura, T., Franco, S., Real, J., et al. Short-term interaction between silent and devastating earthquakes in Mexico. *Nature communications*, 12(1): 2171, 2021. doi: 10.1038/s41467-021-22326-6.

Dragert, H., Wang, K., and James, T. S. A silent slip event on the deeper Cascadia subduction interface. *Science*, 292(5521): 1525–1528, 2001. doi: 10.1126/science.1060152.

Frank, W. B. and Brodsky, E. E. Daily measurement of slow slip from low-frequency earthquakes is consistent with ordinary earthquake scaling. *Science advances*, 5(10):eaaw9386, 2019. doi: 10.1126/sciadv.aaw9386.

Frank, W. B. and Shapiro, N. M. Automatic Detection of Low-Frequency Earthquakes (LFEs) Based on a Beamformed Network Response. *Geophysical Journal International*, 197(2): 1215–1223, May 2014. doi: 10.1093/gji/ggu058.

Frank, W. B., Shapiro, N. M., Husker, A. L., Kostoglodov, V., Romanenko, A., and Campillo, M. Using Systematically Characterized Low-Frequency Earthquakes as a Fault Probe in Guerrero, Mexico. *Journal of Geophysical Research: Solid Earth*, 119(10): 7686–7700, 2014. doi: 10.1002/2014JB011457.

Geological Survey of Canada. Portable Observatories for Lithospheric Analysis and Research Investigating Seismicity (POLARIS), 2000. https://fdsn.org/networks/detail/PO/.

Gombert, B. and Hawthorne, J. C. Rapid Tremor Migration During Few Minute-Long Slow Earthquakes in Cascadia. *Journal of Geophysical Research: Solid Earth*, 128(2):e2022JB025034, 2023. doi: 10.1029/2022JB025034.

González-Vidal, D., Moreno, M., Sippl, C., Baez, J. C., Ortega-Culaciati, F., Lange, D., Tilmann, F., Socquet, A., Bolte, J., Hormazabal, J., et al. Relation between oceanic plate structure, patterns of interplate locking and microseismicity in the 1922 Atacama seismic gap. *Geophysical Research Letters*, 50(15): e2023GL103565, 2023. doi: 10.1029/2023GL103565.

Ide, S., Beroza, G. C., Shelly, D. R., and Uchide, T. A Scaling Law for Slow Earthquakes. *Nature*, 447(7140):76–79, May 2007a. doi: 10.1038/nature05780.

Ide, S., Shelly, D. R., and Beroza, G. C. Mechanism of deep low frequency earthquakes: Further evidence that deep nonvolcanic tremor is generated by shear slip on the plate interface. *Geophysical Research Letters*, 34(3), 2007b. doi: 10.1029/2006GL028890.

Imanishi, K., Uchide, T., and Takeda, N. Determination of focal mechanisms of nonvolcanic tremor using S wave polarization data corrected for the effects of anisotropy. *Geophysical Research Letters*, 43(2):611–619, 2016. doi: 10.1002/2015GL067249.

IRIS Transportable Array. USArray Transportable Array, 2003. doi: 10.7914/SN/TA.

Japan Meteorological Agency. The Seismological Bulletin of Japan, 2023. http://www.data.jma.go.jp/svd/eqev/data/bulletin/index_e.html.

Kao, H., Shan, S.-J., Dragert, H., Rogers, G., Cassidy, J. F., and Ramachandran, K. A Wide Depth Distribution of Seismic Tremors along the Northern Cascadia Margin. *Nature*, 436 (7052):841–844, Aug. 2005. doi: 10.1038/nature03903.

Lin, J.-T., Thomas, A., Bachelot, L., Toomey, D., Searcy, J., and Melgar, D. Detection of Hidden Low-Frequency Earthquakes in Southern Vancouver Island with Deep Learning. *EarthArxiv*, Oct. 2023. doi: 10.31223/x5pm4b.

Lomax, A., Virieux, J., Volant, P., and Berge-Thierry, C. Probabilistic earthquake location in 3D and layered models: Introduction of a Metropolis-Gibbs method and comparison with linear locations. *Advances in seismic event location*, pages 101–134, 2000. doi: 10.1007/978-94-015-9536-0_5.

Lowry, A. R., Larson, K. M., Kostoglodov, V., and Bilham, R. Transient fault slip in Guerrero, southern Mexico. *Geophysical Research Letters*, 28(19):3753–3756, 2001. doi: 10.1029/2001GL013238.

Michel, S., Gualandi, A., and Avouac, J.-P. Interseismic coupling and slow slip events on the Cascadia megathrust. *Pure and Applied Geophysics*, 176:3867–3891, 2019. doi: 10.1007/s00024-018-1991-x.

Michelini, A., Cianetti, S., Gaviano, S., Giunchi, C., Jozinović, D., and Lauciani, V. INSTANCE–the Italian seismic dataset for machine learning. *Earth System Science Data*, 13(12):5509–5544, 2021. doi: 10.5194/essd-13-5509-2021.

Mouchon, C., Frank, W. B., Radiguet, M., Poli, P., and Cotte, N. Subdaily Slow Fault Slip Dynamics Captured by Low-Frequency Earthquakes. *AGU Advances*, 4(4):e2022AV000848, 2023. doi: 10.1029/2022AV000848.

Moutote, L., Itoh, Y., Lengliné, O., Duputel, Z., and Socquet, A. Evidence of a transient aseismic slip driving the 2017 Valparaiso earthquake sequence, from foreshocks to aftershocks. *Journal of Geophysical Research: Solid Earth*, page e2023JB026603, 2023. doi: 10.1029/2023JB026603.

Münchmeyer, J. PyOcto: A high-throughput seismic phase associator. *Seismica*, 3(1), 2024. doi: 10.26443/seismica.v3i1.1130.

Münchmeyer, J., Woollam, J., Rietbrock, A., Tilmann, F., Lange, D., Bornstein, T., Diehl, T., Giunchi, C., Haslinger, F., Jozinović, D., et al. Which picker fits my data? A quantitative evaluation of deep learning based seismic pickers. *Journal of Geophysical Research: Solid Earth*, 127(1):e2021JB023499, 2022. doi: 10.1029/2021JB023499.

Natural Resources Canada. Canadian National Seismograph Network, 1975. doi: 10.7914/SN/CN.

Natural Resources Canada. Canadian Seismic Research Network, 2002. https://fdsn.org/networks/detail/C8/.

Northern California Earthquake Data Center. Berkeley Digital Seismic Network (BDSN), 2014a. doi: 10.7932/BDSN.

Northern California Earthquake Data Center. High Resolution Seismic Network (HRSN), 2014b. doi: 10.7932/HRSN.

Okada, Y., Nishimura, T., Tabei, T., Matsushima, T., and Hirose, H. Development of a detection method for short-term slow slip events using GNSS data and its application to the Nankai subduction zone. *Earth, Planets and Space*, 74(1):1–18, 2022. doi: 10.1186/s40623-022-01576-8.

Ozawa, S., Murakami, M., Kaidzu, M., Tada, T., Sagiya, T., Hatanaka, Y., Yarai, H., and Nishimura, T. Detection and monitoring of ongoing aseismic slip in the Tokai region, central Japan. *Science*, 298(5595):1009–1012, 2002. doi: 10.1126/science.1076780.

Radiguet, M., Perfettini, H., Cotte, N., Gualandi, A., Valette, B., Kostoglodov, V., Lhomme, T., Walpersdorf, A., Cabral Cano, E., and Campillo, M. Triggering of the 2014 M w 7.3 Papanoa earthquake by a slow slip event in Guerrero, Mexico. *Nature Geoscience*, 9 (11):829–833, 2016. doi: 10.1038/ngeo2817.

Ronneberger, O., Fischer, P., and Brox, T. U-net: Convolutional networks for biomedical image segmentation. In *Medical Image Computing and Computer-Assisted Intervention–MICCAI 2015: 18th International Conference, Munich, Germany, October 5-9, 2015, Proceedings, Part III 18*, pages 234–241. Springer, 2015. doi: 10.1007/978-3-319-24574-4_28.

Ross, Z. E., Meier, M.-A., Hauksson, E., and Heaton, T. H. Generalized seismic phase detection with deep learning. *Bulletin of the Seismological Society of America*, 108(5A):2894–2901, 2018. doi: 10.1785/0120180080.

Rouet-Leduc, B., Hulbert, C., McBrearty, I. W., and Johnson, P. A. Probing slow earthquakes with deep learning. *Geophysical research letters*, 47(4):e2019GL085870, 2020. doi: 10.1029/2019GL085870.

Royer, A. and Bostock, M. A comparative study of low frequency earthquake templates in northern Cascadia. *Earth and Planetary Science Letters*, 402:247–256, 2014. doi: 10.1016/j.epsl.2013.08.040.

Rubin, A. M. and Armbruster, J. G. Imaging Slow Slip Fronts in Cascadia with High Precision Cross-Station Tremor Locations. *Geochemistry, Geophysics, Geosystems*, 14(12):5371–5392, 2013. doi: 10.1002/2013GC005031.

Savard, G. and Bostock, M. G. Detection and Location of Low-Frequency Earthquakes Using Cross-Station Correlation. *Bulletin of the Seismological Society of America*, 105(4):2128–2142, June 2015. doi: 10.1785/0120140301.

Shelly, D. R. Migrating tremors illuminate complex deformation beneath the seismogenic San Andreas fault. *Nature*, 463(7281): 648–652, 2010. doi: 10.1038/nature08755.

Shelly, D. R. A 15 Year Catalog of More than 1 Million Low-Frequency Earthquakes: Tracking Tremor and Slip along the Deep San Andreas Fault. *Journal of Geophysical Research: Solid Earth*, 122(5):3739–3753, 2017. doi: 10.1002/2017JB014047.

Shelly, D. R., Beroza, G. C., and Ide, S. Non-Volcanic Tremor and Low-Frequency Earthquake Swarms. *Nature*, 446(7133): 305–307, Mar. 2007. doi: 10.1038/nature05666.

Shelly, D. R., Ellsworth, W. L., Ryberg, T., Haberland, C., Fuis, G. S., Murphy, J., Nadeau, R. M., and Bürgmann, R. Precise Location of San Andreas Fault Tremors near Cholame, California Using Seismometer Clusters: Slip on the Deep Extension of the Fault? *Geophysical Research Letters*, 36(1), 2009. doi: 10.1029/2008GL036367.

Socquet, A., Valdes, J. P., Jara, J., Cotton, F., Walpersdorf, A., Cotte, N., Specht, S., Ortega-Culaciati, F., Carrizo, D., and Norabuena, E. An 8 Month Slow Slip Event Triggers Progressive Nucleation of the 2014 Chile Megathrust. *Geophysical Research Letters*, 44 (9):4046–4053, 2017. doi: 10.1002/2017GL073023.

Supino, M., Poiata, N., Festa, G., Vilotte, J. P., Satriano, C., and Obara, K. Self-Similarity of Low-Frequency Earthquakes. *Scientific Reports*, 10(1):6523, Apr. 2020. doi: 10.1038/s41598-020-63584-6.

Tan, Y. J., Waldhauser, F., Ellsworth, W. L., Zhang, M., Zhu, W., Michele, M., Chiaraluce, L., Beroza, G. C., and Segou, M. Machine-learning-based high-resolution earthquake catalog reveals how complex fault structures were activated during the 2016–2017 Central Italy sequence. *The Seismic Record*, 1(1): 11–19, 2021. doi: 10.1785/0320210001.

Thomas, A. M., Inbal, A., Searcy, J., Shelly, D. R., and Bürgmann, R. Identification of low-frequency earthquakes on the San Andreas Fault with deep learning. *Geophysical Research Letters*, 48(13): e2021GL093157, 2021. doi: 10.1029/2021GL093157.

UNAVCO, United States of America. Plate Boundary Observatory Borehole Seismic Network (PBO), 2004. https://fdsn.org/networks/detail/PB/.

USGS Menlo Park. USGS Northern California Seismic Network, 1966. doi: 10.7914/SN/NC.

Wang, Q.-Y., Frank, W. B., Abercrombie, R. E., Obara, K., and Kato, A. What makes low-frequency earthquakes low frequency. *Science Advances*, 9(32):eadh3688, 2023. doi: 10.1126/sciadv.adh3688.

Wech, A. G. Cataloging Tectonic Tremor Energy Radiation in the Cascadia Subduction Zone. *Journal of Geophysical Research: Solid Earth*, 126(10):e2021JB022523, 2021. doi: 10.1029/2021JB022523.

Woollam, J., Münchmeyer, J., Tilmann, F., Rietbrock, A., Lange, D., Bornstein, T., Diehl, T., Giunchi, C., Haslinger, F., Jozinović, D., et al. SeisBench—A toolbox for machine learning in seismology. *Seismological Research Letters*, 93(3):1695–1709, 2022. doi: 10.1785/0220210324.

Zhu, W. and Beroza, G. C. PhaseNet: A deep-neural-network-based seismic arrival-time picking method. *Geophysical Journal International*, 216(1):261–273, 2019. doi: 10.1093/gji/ggy423.